REPORT DOCUMENTATION PAGE

Form Approved
OMB No. 0704-0188

PLEASE DO NOT RETURN YOUR FORM TO THE ABOVE ORGANIZATION.

1. REPORT DATE *(DD-MM-YYYY)*	2. REPORT TYPE	3. DATES COVERED *(From - To)*
29-04-2015	Journal Article	

4. TITLE AND SUBTITLE

High-resolution and fast-response fiber-optic temperature sensor using silicon Fabry-Pérot cavity

5a. CONTRACT NUMBER

5b. GRANT NUMBER

5c. PROGRAM ELEMENT NUMBER

0601153N

6. AUTHOR(S)

Guigen Liu, Ming Han, and Weilin Hou

5d. PROJECT NUMBER

5e. TASK NUMBER

5f. WORK UNIT NUMBER

73-4951-05-5

7. PERFORMING ORGANIZATION NAME(S) AND ADDRESS(ES)

Naval Research Laboratory
Oceanography Division
Stennis Space Center, MS 39529-5004

8. PERFORMING ORGANIZATION REPORT NUMBER

NRL/JA/7330-15-2519

9. SPONSORING/MONITORING AGENCY NAME(S) AND ADDRESS(ES)

Office of Naval Research
One Liberty Center
875 North Randolph Street, Suite 1425
Arlington, VA 22203-1995

10. SPONSOR/MONITOR'S ACRONYM(S)

ONR

11. SPONSOR/MONITOR'S REPORT NUMBER(S)

12. DISTRIBUTION/AVAILABILITY STATEMENT

Approved for public release, distribution is unlimited.

13. SUPPLEMENTARY NOTES

14. ABSTRACT

We report a fiber-optic sensor based on a silicon Fabry-Pérot cavity, fabricated by attaching a silicon pillar on the tip of a single-mode fiber, for high-resolution and high-speed temperature measurement. The large thermo-optic coefficient and thermal expansion coefficient of the silicon material give rise to an experimental sensitivity of 84.6 pm/°C. The excellent transparency and large refractive index of silicon over the infrared wavelength range result in a visibility of 33 dB for the reflection spectrum. A novel average wavelength tracking method has been proposed and demonstrated for sensor demodulation with improved signal-to-noise ratio, which leads to a temperature resolution of 6 × 10⁻⁴ °C. Due to the high thermal diffusivity of silicon, a response time as short as 0.51 ms for a sensor with an 80-μm-diameter and 200-μm-long silicon pillar has been experimentally achieved, suggesting a maximum frequency of ~2 kHz can be reached, to address the needs for highly dynamic environmental variations such as those found in the ocean.

15. SUBJECT TERMS

Fiber optics sensors; Thermal effects; Interferometry

16. SECURITY CLASSIFICATION OF:			17. LIMITATION OF ABSTRACT	18. NUMBER OF PAGES	19a. NAME OF RESPONSIBLE PERSON
a. REPORT	b. ABSTRACT	c. THIS PAGE			Weilin Hou
Unclassified	Unclassified	Unclassified	UU	11	19b. TELEPHONE NUMBER *(Include area code)* (228) 688-5257

Reset

Standard Form 298 (Rev. 8/98)
Prescribed by ANSI Std. Z39.18

15-1231-0943

PUBLICATION OR PRESENTATION RELEASE REQUEST

Publication 9602 RLINST 5510.40

1. REFERENCES AND ENCLOSURES

Ref: (a) NRL Instruction 5600.2
(b) NRL Instruction 5510.40E

Encl: (1) Two copies of subject publication/presentation

2. TYPE OF PUBLICATION OR PRESENTATION

( ) Abstract only, published	( ) Abstract only, not published
( ) Book author	( ) Book chapter
( ) Book editor	( ) Multimedia report
( ) Conference Proceedings (refereed)	( ) Conference Proceedings (not refereed)
(X) Journal article (refereed)	( ) Journal article (not refereed)
( ) Oral Presentation, published	( ) Oral Presentation, not published
( ) Video ( ) Poster	( ) Other, explain

ALL DOCUMENTS/PRESENTATIONS MUST BE ATTACHE

3. ADMINISTRATIVE INFORMATION

STRN NRL/JA/7330-15-2519
Route Sheet No. 7330/
Job Order No. 73-4951-05-5
Classification U S C
FOUO ____
Sponsor ONR BASE 6.1-
Sponsor's approval ____ yes* (attached)
(*Required if research is otheran 6.1/6.2 NRL or ONR unclassified research or if publication/presentation is classified

4. AUTHOR

Title of Paper or Presentation
High-resolution and fast-response fiber-optic temperature sensor using silicon Fabry-Perot cavity

AUTHOR(s) LEGAL NAMES(s) OF RECORD (First, MI, Last), CODE, (Affiliation if not NRL).
Guigen Liu Universtiy of Nebraska-Lincoln, Ming Han University of Nebraka-Lincoln, Weilin Hou 7333,

This paper will be presented at the Optics Express
(Name of Conference)
(Date, Place and Classification of Conference)

and/or for published in Optics Express, Unclassified
(Name and Classification of Publication) (Name of Publisher)

5. CERTIFICATION OR CLASSIFICATION

It is my opinion that the subject paper (is ____) (is not __x__) classified, in accordance with reference (b) and this paper does not violate any disclosure of trade secrets or suggestions of outside individuals or concerns which have been communicated to the NRL in confidence.

This subject paper (has ____) (has never __x__) been incorporated in an official NRL Report.

Weilin Hou, 7333 (Signature)
Name and Code (Principal Author) (Legal Name of Record and Signature Only)

6. ROUTING/APPROVAL (NOTE: If name other than your legal name of record is used on the publication or presentation itself, add an explanatory note in the "comments" section below next to your signed legal name of record.)

CODE	SIGNATURE	DATE	COMMENTS
Co-Author(s) Weilin Hou, 7333		3/18/15	Need by 1 April 2015
			This is a Final Security Review. Any changes made in the document, after approved by Code 1231, nullify the Security Review.
Section Head			
Branch Head Richard L. Crout, 7330		3-18-2015	
Division Head Ruth H. Preller, 7300		3-18-15	1. To the best knowledge of this Division, the subject matter of this publication (has ____)(has never ____ X)been classified. 2. This paper (does ____) (does not __X__) contain any militarily critical technology.
ADOR/Director NCST E. R. Franchi, 7000			
DOR/CO			
Security, Code 1231		3/23/15	A copy of the paper, abstract or presentation is filed in this office
Associate Counsel,Code 1008.3	Chris and Beede invention-memo		- 3/31/2015
Public Affairs (Unclassified/ Unlimited Only), Code 7030.4	Shannon Mensi	3-30-15	
Division, Code			
Author, Code			

HQ-NRL 5511/6 (Rev. 12/14) THIS FORM CANCELS AND SUPERSEDES ALL PREVIOUS VERSIONS

High-resolution and fast-response fiber-optic temperature sensor using silicon Fabry-Pérot cavity

Guigen Liu,[1] Ming Han,[1,*] and Weilin Hou[2]

[1]*Department of Electrical Engineering, University of Nebraska-Lincoln, Lincoln, NE 68588, USA*
[2]*Naval Research Laboratory, Code 7333, Stennis Space Center, MS 39529, USA*
[*]*mhan@unl.edu*

Abstract: We report a fiber-optic sensor based on a silicon Fabry-Pérot cavity, fabricated by attaching a silicon pillar on the tip of a single-mode fiber, for high-resolution and high-speed temperature measurement. The large thermo-optic coefficient and thermal expansion coefficient of the silicon material give rise to an experimental sensitivity of 84.6 pm/°C. The excellent transparency and large refractive index of silicon over the infrared wavelength range result in a visibility of 33 dB for the reflection spectrum. A novel average wavelength tracking method has been proposed and demonstrated for sensor demodulation with improved signal-to-noise ratio, which leads to a temperature resolution of 6×10^{-4} °C. Due to the high thermal diffusivity of silicon, a response time as short as 0.51 ms for a sensor with an 80-μm-diameter and 200-μm-long silicon pillar has been experimentally achieved, suggesting a maximum frequency of ~2 kHz can be reached, to address the needs for highly dynamic environmental variations such as those found in the ocean.

OCIS codes: (060.2370) Fiber optics sensors; (120.6810) Thermal effects; (120.3180) Interferometry.

References and links

1. Y. J. Rao, "In-fibre Bragg grating sensors," Meas. Sci. Technol. **8**(4), 355–375 (1997).
2. D. Zhang, J. Wang, Y. Wang, and X. Dai, "A fast response temperature sensor based on fiber Bragg grating," Meas. Sci. Technol. **25**(7), 075105 (2014).
3. S. Bandyopadhyay, J. Canning, M. Stevenson, and K. Cook, "Ultrahigh-temperature regenerated gratings in boron-codoped germanosilicate optical fiber using 193 nm," Opt. Lett. **33**(16), 1917–1919 (2008).
4. S. Khaliq, S. W. James, and R. P. Tatam, "Enhanced sensitivity fibre optic long period grating temperature sensor," Meas. Sci. Technol. **13**(5), 792–795 (2002).
5. A. M. Hatta, G. Rajan, Y. Semenova, and G. Farrell, "SMS fibre structure for temperature measurement using a simple intensity-based interrogation system," Electron. Lett. **45**(21), 1069–1070 (2009).
6. Y. B. Zhang, G. R. Pickrell, B. Qi, A. Safaai-Jazi, and A. Wang, "Single-crystal sapphire-based optical high-temperature sensor for harsh environments," Opt. Eng. **43**(1), 157–164 (2004).
7. G. Coviello, V. Finazzi, J. Villatoro, and V. Pruneri, "Thermally stabilized PCF-based sensor for temperature measurements up to 1000 degrees C," Opt. Express **17**(24), 21551–21559 (2009).
8. P. F. Wang, M. Ding, L. Bo, C. Y. Guan, Y. Semenova, Q. Wu, G. Farrell, and G. Brambilla, "Fiber-tip high-temperature sensor based on multimode interference," Opt. Lett. **38**(22), 4617–4620 (2013).
9. M. Ding, P. Wang, and G. Brambilla, "Fast-response high-temperature microfiber coupler tip thermometer," IEEE Photon. Technol. Lett. **24**(14), 1209–1211 (2012).
10. I. Kajanto and A. T. Friberg, "A silicon-based fibre-optic temperature sensor," J. Phys. E Sci. Instrum. **21**(7), 652–656 (1988).
11. L. Schultheis, H. Amstutz, and M. Kaufmann, "Fiber-optic temperature sensing with ultrathin silicon étalons," Opt. Lett. **13**(9), 782–784 (1988).
12. J. W. Berthold III, S. E. Reed, and R. G. Sarkis, "Reflective fiber optic temperature sensor using silicon thin film," Opt. Eng. **30**(5), 524–528 (1991).
13. G. Cocorullo, F. G. D. Corte, M. Iodice, I. Rendina, and P. M. Sarro, "A temperature all-silicon micro-sensor based on the thermo-optic effect," IEEE T. Electron Dev. **44**(5), 766–774 (1997).

#232621 - $15.00 USD Received 16 Jan 2015; revised 2 Mar 2015; accepted 4 Mar 2015; published 10 Mar 2015

14. W. Hou, S. Woods, E. Jarosz, W. Goode, and A. Weidemann, "Optical turbulence on underwater image degradation in natural environments," Appl. Opt. **51**(14), 2678–2686 (2012).
15. W. Hou, *Ocean Sensing and Monitoring* (SPIE Press, 2013).
16. J. Komma, C. Schwarz, G. Hofmann, D. Heinert, and R. Nawrodt, "Thermo-optic coefficient of silicon at 1550 nm and cryogenic temperatures," Appl. Phys. Lett. **101**(4), 041905 (2012).
17. F. W. Guo, T. Fink, M. Han, L. Koester, J. Turner, and J. S. Huang, "High-sensitivity, high-frequency extrinsic Fabry-Perot interferometric fiber-tip sensor based on a thin silver diaphragm," Opt. Lett. **37**(9), 1505–1507 (2012).
18. I. M. White and X. D. Fan, "On the performance quantification of resonant refractive index sensors," Opt. Express **16**(2), 1020–1028 (2008).
19. M. N. Özişik, *Heat Transfer A Basic Approach* (McGraw-Hill, 1985).
20. W. Qu, G. M. Mala, and D. Li, "Heat transfer for water flow in trapezoidal silicon microchannels," Int. J. Heat Mass Transfer **43**(21), 3925–3936 (2000).

1. Introduction

It is of great importance to monitor the temperature in a variety of industries, such as food inspection, pharmacy, oil/gas exploration, environment, and high-voltage power systems. Fiber-optic temperature sensors have been the focus of intensive research owning to their many advantages, such as small size, light weight, immunity to electromagnetic interference, harsh environment tolerance, remote sensing capability, and capability for distributed or quasi-distributed measurement. A number of sensor structures, including fiber Bragg gratings (FBGs) [1–3], long period gratings [4], and various forms of interferometers [5–8], have been developed and studied for temperature measurement with reduced cost, increased sensitivity, or enhanced temperature range.

In addition to sensitivity and temperature range, temperature resolution and speed (or response time) are another two important sensor parameters, which have not been fully studied. Temperature resolution, defined as the minimum detectable temperature changes, is determined by both the sensor sensitivity (defined as the sensor output from a given temperature change) and the noise of the sensor system; while the response time is mostly limited by the time constant of the heat transfer process between the sensing element and the surrounding environment. The sensing element of many fiber-optic temperature sensors is part of the fiber itself, which is made of fused silica. The temperature resolution and the speed are limited by the relatively low thermo-optic coefficient (TOC) and thermal diffusivity of the glass material that lead, respectively, to reduced sensor sensitivity and increased time for the temperature of the sensing element to reach equilibrium with the surrounding environment. For example, it is well-known that an FBG, whose reflection spectrum features a single reflection peak, exhibit a temperature sensitivity of ~10 pm/°C. A fiber modal interferometer based on a single mode-multimode-single mode fiber structure has been reported to have a temperature resolution of 0.2 °C [5]. Obviously, many of the reported all-silica-fiber-based temperature sensors possess relatively low sensitivity and relatively low temperature resolution. As to the response time, the package of a FBG with a copper tube encapsulation can greatly reduce the response time of the sensor from several seconds to 48.6 ms in water [2]. A response time of 16 ms in air was also demonstrated for a microfiber coupler tip temperature sensor [9].

Compared to fused silica, crystalline silicon is a much more desirable sensor material for high-resolution and high-speed temperature sensing. Silicon is highly transparent over the infrared wavelength and has a TOC approximately 10 times larger than that of fused silica used for the sensing element for most fiber-optic sensors, resulting in potentially much higher temperature sensitivity. In addition, silicon-based temperature sensor also potentially has high speed because of the large thermal diffusivity of silicon, which is comparable to many metals (e.g., aluminum and gold) and more than 60 times larger than fused silica. However, to date, only a few papers have reported on the use of silicon as temperature sensing element [10–13] and the potential of silicon has not been fully explored for high-resolution and high-speed temperature sensing. In [10], the dependence of the absorption of a silicon film on

#232621 - $15.00 USD Received 16 Jan 2015; revised 2 Mar 2015; accepted 4 Mar 2015; published 10 Mar 2015

temperature was used for temperature sensing and the sensor showed relatively low temperature resolution of ± 0.12 °C and a long response time on the order of 1 s. A simpler structure with a thin silicon film (thickness < 1 μm) deposited directly on the fiber end through electron-beam evaporation was demonstrated in [11], with a temperature resolution of only 3 °C. The radio-frequency sputtering was applied in [12] to simplify the deposition process. The resolution was mainly limited by the small thickness of the silicon film that led to broad spectral fringes. Instead of silicon film, a silicon micro-waveguide patterned on a micro-electro-mechanical system (MEMS) was developed as temperature sensor [13]. Due to the increased length of the Si sensing element, the temperature resolution was improved to 0.064 °C. However, it is a challenge to integrate the fiber and the MEMS into a single sensor device and the large size of the sensing element also limits its temperature measurement speed.

In this paper, we propose and demonstrate a high-resolution and high-speed fiber-optic temperature sensor by attaching a small double-side-polished silicon pillar to the fiber tip that forms a Fabry-Pérot (FP) cavity. The diameter of the pillar is 80 μm or 100 μm, smaller than the fiber diameter, leading to fast temperature response. The length of the pillar is ~200 μm, much thicker than the previously reported thin films deposited on the fiber endface, which, together with the large refractive index (RI) of the silicon material, results in dense fringes in the reflection spectrum of the FP cavity. Using this unique spectral characteristic of the sensor, we developed a novel data processing method to significantly reduce the noise and improve the measurement resolution. We also theoretically and experimentally investigate the response time of the sensor. Our results show that the sensor described in this paper features a high temperature resolution of 6×10^{-4} °C and a short response time of 0.51 ms. The developed high-resolution and fast-response thermometer will serve as a promising tool in the precise and real-time characterization of temperature structure in highly dynamic optical turbulence, which is one of the key issues of underwater imaging in oceanography [14, 15].

2. Sensor system and sensor fabrication

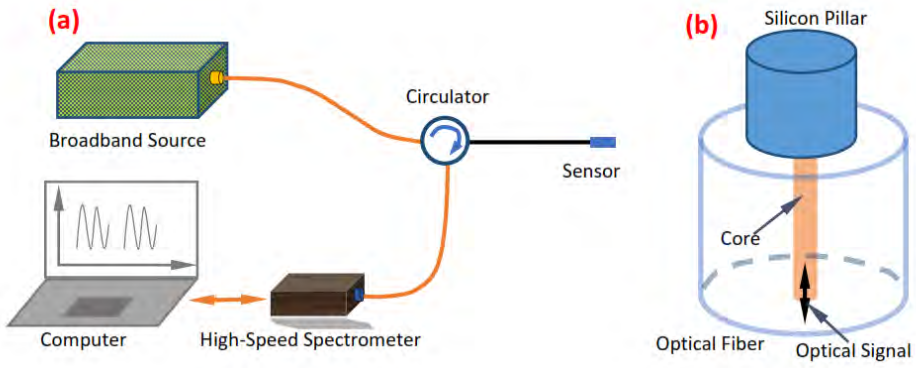

Fig. 1. Schematic diagram of (a) the system and (b) the sensor head in detail.

The sensor system is schematically shown in Fig. 1(a). Through a fiber-optic circulator, a white light source is injected into the sensor head and the returned signal is directed to a high-speed spectrometer that is based on a transmission grating and a diode array operating in the 1550 nm wavelength window. The sensor head is schematically shown in Fig. 1(b), which consists of a ~200 μm long double-side-polished silicon pillar attached to the endface of a signal mode fiber (SMF). The wavelength of the N^{th} fringe peak, λ_N, of the reflection spectrum is given as

$$\left(N + \frac{1}{2}\right)\lambda_N = 2nL, \tag{1}$$

#232621 - $15.00 USD Received 16 Jan 2015; revised 2 Mar 2015; accepted 4 Mar 2015; published 10 Mar 2015

where n and L are, respectively, the RI and cavity length of the FP cavity. Both n and L are dependent on temperature, due to the thermo-optic effect and the thermal expansion of the silicon material. Therefore temperature change can be measured by monitoring λ_N. From Eq. (1), the temperature sensitivity is given by

$$\frac{\partial \lambda_N}{\partial T} = \lambda_N \left(\frac{1}{n}\frac{\partial n}{\partial T} + \frac{1}{L}\frac{\partial L}{\partial T} \right). \tag{2}$$

The sensitivity depends on the TOC and the thermo-expansion coefficient (TEC) of the sensing material. The TOC and TEC for silicon are, respectively, 1.5×10^{-4} RIU/°C and 2.55×10^{-6} m/(m·°C) at 25 °C. To estimate the sensitivity, these values are applied to Eq. (2) at the peak wavelength λ_N around 1550 nm and the RI of silicon is assumed to be 3.4 [16]. From this, the sensitivity of the temperature sensor proposed here is estimated to be 72 pm/°C. As a comparison to the all-fiber based sensor, the TOC and TEC for fused silica are, respectively, 1.28×10^{-5} RIU/°C and 5.5×10^{-7} m/(m·°C) at 25°C, both of which are much smaller than those for silicon. Assuming the RI of silica at 1550 nm is 1.5, the sensitivity of an all-fiber based sensor is estimated to be 14 pm/°C, which is more than 5 times smaller than the silicon-based sensor proposed here.

The high RI (~3.4) of silicon over infrared wavelength range produces a high reflectivity at the interfaces between silicon and the surrounding environment and between silicon and the fiber endface, which facilitates to obtain a large optical power and a high fringe-visibility of the interferometric spectrum from the FP cavity for improving the sensor resolution. In addition, the high RI and the relatively long FP cavity yield a large number of fringes within the wavelength range of the spectrometer, which can be exploited to further increase the temperature resolution. More details concerning the sensitivity and resolution are provided in Section 3.

The proposed sensor also features a short response time. Due to the high thermal diffusivity of silicon and the small size of the sensor head, the temperature within the FP cavity can quickly reach equilibrium with surroundings. The response time is studied both theoretically and experimentally in detail in Section 4.

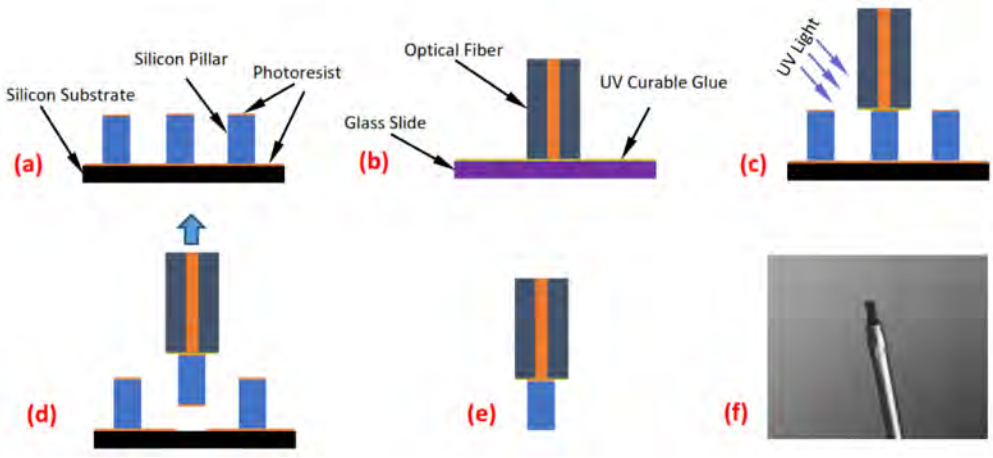

Fig. 2. Sensor fabrication steps. (a) Manufacturing of upstanding silicon pillars through MEMS technology. (b) Attaching a thin film of UV curable glue on the fiber endface. (c) Adjusting and pressing the fiber endface against a silicon pillar and applying UV light to cure the glue. (d) Lifting up the cured sensor head. (e) Removing the residual photoresist by rinsing it with alcohol. (f) Optical microscope of a fabricated sensor head with an 80-μm-diameter and 200-μm-long silicon pillar.

#232621 - $15.00 USD Received 16 Jan 2015; revised 2 Mar 2015; accepted 4 Mar 2015; published 10 Mar 2015

The fabrication steps to construct a sensor head shown in Fig. 1(b) are described in Fig. 2. The fabrication started with bonding a 200-μm-thick double-side-polished silicon wafer on top of another larger silicon wafer through a layer of photoresist. The larger silicon wafer was used as a substrate to facilitate the fabrication and later as a support for the fabricated silicon pillars. Then another layer of photoresist was coated on the top of the 200-μm-thick wafer and patterned according. The patterned top silicon layer was etched all the way to the substrate using deep-reactive-ion-etching, leaving the upstanding silicon pillars attached to the substrate. A thin film of UV-curable glue was spin-coated on a piece of glass substrate and the glue was transferred to the cleaved and cleaned endface of a piece of SMF by pressing the fiber endface to the glue film on the glass substrate [17], as shown in Fig. 2(b). Then, under optical microscope, the fiber endface with glue was adjusted and pressed onto one of the upstanding silicon pillars, and the UV glue was cured by UV irradiation, as shown in Fig. 2(c). After the glue was cured, the fiber with a silicon pillar attached was lifted up from the substrate, as shown in Fig. 2(d). Finally, the fabrication is completed by cleaning the residual photoresist on the end of the pillar with alcohol, as shown in Fig. 2(e). Due to the ultra-thin thickness of residual photoresist between SMF and silicon pillar, the reflection spectrum of the silicon FP cavity was not affected. One of the fabricated sensor heads is shown in Fig. 2(f), in which the diameter and length of the silicon pillar are 80 μm and 200 μm, respectively.

3. Sensitivity and resolution

3.1 Experimental study of sensitivity to temperature

Figure 3(a) shows the reflection spectrum at wavelength around 1550 nm of the sensor measured with a high-resolution optical sensor interrogator (Model: sm125, Micron Optics), indicating a fringe visibility as high as 33 dB and a free spectrum range of 1.46 nm. The temperature response of the sensor was experimentally studied by placing the sensor in a furnace and the wavelength position of the fringe valley near 1550 nm in Fig. 3(a) was monitored as the temperature increased. The results are shown in Fig. 3(b). The good linear response of the wavelength to temperature suggests a temperature sensitivity of 84.6 pm/°C of the sensor over the temperature range from 20 °C to 100°C, which is close to the theoretical value of 72 pm/°C obtained in Section 2. The small discrepancy between the experimental and theoretical values may be attributed to the potentially underestimated TOC and TEC and the ignorance of the wavelength-dependent RI of silicon.

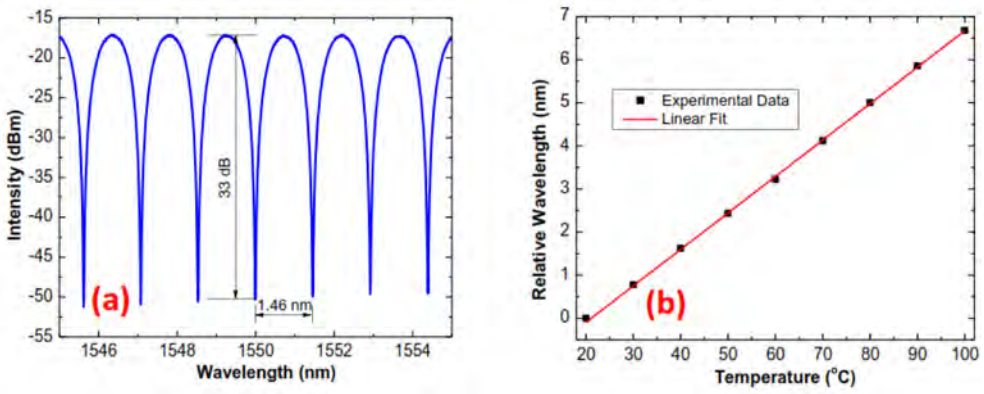

Fig. 3. (a) Reflection spectrum of the sensor. (b) Relative wavelength shift versus temperature.

3.2 Wavelength noise and temperature resolution

In addition to the high sensitivity discussed in Section 3.1, low noise in determining the wavelength positions of fringe valleys is also essential for high temperature resolution. In our

#232621 - $15.00 USD Received 16 Jan 2015; revised 2 Mar 2015; accepted 4 Mar 2015; published 10 Mar 2015

experiment, the high-speed spectrometer (Model: I-MON 256 USB, Ibsen, Denmark), based on a transmission grating that spreads the wavelength spectrum spatially on a detector array, is capable of measuring the spectrum at a line scan rate of 6 kHz over the wavelength range from 1525 – 1570 nm. The detector array has 256 pixels; therefore each spectral frame consists of 256 data points that are approximately evenly spaced over the wavelength range. Due to the large RI of the silicon material and the large FP cavity length, the reflection spectrum of the sensor consists of a large number of fringes, as shown in Fig. 4(a). For sensors based on FBGs, FP cavities or other optical resonators [18], wavelength tracking method is typically used for signal demodulation, where the wavelength position of a single spectral feature, such as a fringe valley, a fringe peak, or a spectral notch, is used to gauge the measurands. Here, making use of the large number of fringes of the sensor, we propose and demonstrate an average wavelength tracking method that can significantly improve the noise performance and the temperature resolution of the sensor.

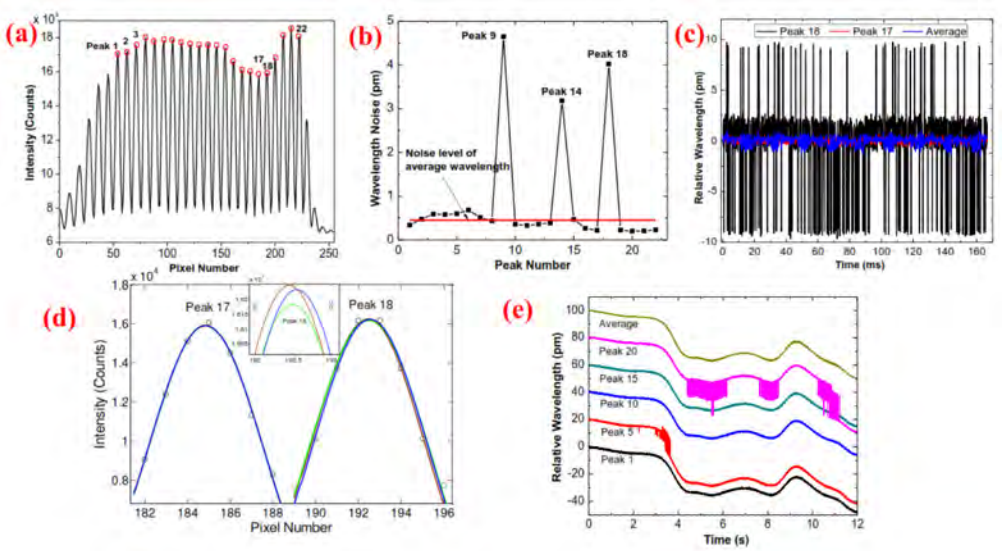

Fig. 4. (a) A frame of the reflection spectrum measured by the high-speed spectrometer. (b) Wavelength noise of each peak shown in (a), the red line represents the noise level of the average fringe peak wavelength. (c) Fitted peak wavelength for peaks 17 and 18 and the average wavelength versus time. (d) Three frames of data for peaks 17 and 18 that are used for peak wavelength fitting. Inset is a close-up view of data fitting for peak 18. (e) Relative wavelength evolution during natural cooling of hot water for five peaks and the average wavelength. Note that the positions of peaks are moved vertically for clear comparison of noise in (e).

For demonstration, 6000 continuous spectral frames are obtained in 1 s when the sensor is under constant ambient temperature. The average peak wavelength tracking uses 22 fringe peaks indicated in Fig. 4(a). For each peak on a spectral frame, the data point of local maximum is identified and Gaussian curve fitting is applied to a total of 7 data points centered at the local maximum to find the wavelength position of the fringe peak. While Lorentzian and Gaussian curve fittings are two widely used methods for determining a single peak position, Gaussian fitting is chosen in this work due to the low finesse of the FP interferometer. However, the average wavelength tracking method is feasible no matter what method is applied to do the peak finding. The noise for each fringe peak, defined as the standard deviation (SD) of the fitted peak wavelength positions from the 6000 spectral frames, is shown in Fig. 4(b). It is seen that the fitted peak wavelengths have a small noise except for some singular peaks, i.e. peaks 9, 14, and 18 shown in Fig. 4(a), whose noise levels are approximately 10 times larger than those of the majority “normal” peaks. Instead of using

#232621 - $15.00 USD Received 16 Jan 2015; revised 2 Mar 2015; accepted 4 Mar 2015; published 10 Mar 2015

the wavelength of any single peak, we use the arithmetic average wavelength of all the peaks in a spectral frame to gauge the temperature. The noise of the average wavelength, shown as the red line in Fig. 4(b), is comparable to the noises of the "normal" peaks. For more details, the fitted peak wavelengths for peaks 17 (normal) and 18 (singular) and the average wavelength obtained from all the 22 peaks are compared in Fig. 4(c). The noises for peak 17, peak 18 and average wavelength are 0.219 pm, 4.021 pm and 0.453 pm, respectively. It clearly shows that the average wavelength tracking method used here suppresses the undesirable effect of the singular peaks and the noise is maintained at a low level.

To examine the cause of the large noise level of these singular peaks, Fig. 4(d) shows three frames of data points that are used for Gaussian fitting of peaks 17 (normal peak) and 18 (singular peak). For peak 18, there are two adjacent data points at the top having very close intensity values. As a result, the identification of the data point of local maximum is more sensitive to the data noise and may vary from frame to frame between these adjacent data points due to the data noise. It is found that the fitting peak wavelength shows a large variation when the identified data point of local maximum changes, as in the case for peak 18 shown in more details in the inset to Fig. 4(d). It is impractical to reduce the noise by simply removing the singular peaks in practice because a singular peak at one temperature level may become a normal peak at a different temperature level, and vice versa. The existence of singular peaks is often unpredictable and unavoidable in practice, especially when the resolution of a spectrometer is limited. To verify this, we placed the sensor in a cup of hot water and Fig. 4(e) shows wavelength positions of several peaks of a sensor in response to the natural cooling of the water within a time span of 12 s. It is seen that peaks 1, 10, and 15 are normal peaks, whose fitted wavelengths did not show large variations throughout the experiment. Peaks 5 and 20 experienced transitions between normal and singular as the temperature varied and their noise behavior changed accordingly and significantly. However, the average peak wavelength, also shown in Fig. 4(e), did not exhibit any large noise. Therefore it is verified that the average wavelength tracking method provides an efficient way to suppress large noise from the singular peaks.

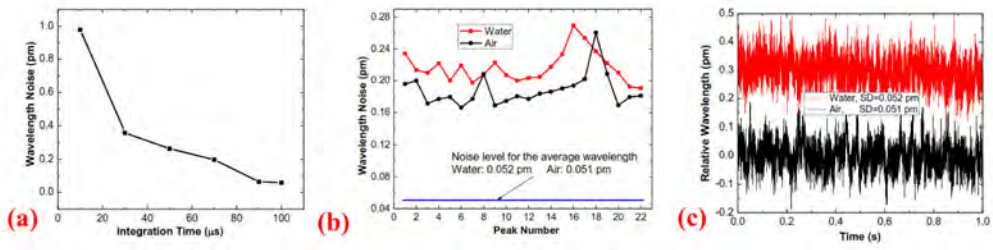

Fig. 5. (a) Wavelength noise with respect to integration time of the spectrometer. (c) Noise of individual peaks when the sensor is placed in water (red) or air (black). The blue line indicates the noise level of the average wavelength. (c) Variations in the average wavelength with time for the sensor placed in water (red) or air (black). Note that the wavelengths are vertically shifted for better view.

In addition to the average wavelength method, it was also discovered that the wavelength noise could be further reduced by increasing the integration time of the spectrometer, as illustrated in Fig. 5(a), which shows the noise of the average wavelength as a function of the integration time. Compared to the noise with integration time of 10 μs (the case for Fig. 4), the noise at 100 μs was reduced by more than 10 times. The improvement of the noise performance is due to the improved signal-to-noise ratio (SNR) of the spectrum obtained with longer integration time. Furthermore, it was also observed that a higher visibility of the reflection spectrum helped reduce the noise. With improved SNR, the number of the singular fringe peaks with large noise can be reduced or even eliminated under certain conditions. However, even for the case where no singular peaks are present, the average wavelength

#232621 - $15.00 USD Received 16 Jan 2015; revised 2 Mar 2015; accepted 4 Mar 2015; published 10 Mar 2015

tracking method can still reduce the measurement noise by approximately a factor of $\sqrt{M}$, where M is the number of peaks that are used for calculating the average wavelength. As an example, Fig. 5(b) shows the noises of individual peak wavelengths and the average peak wavelength for a sensor with a visibility of 33 dB when the integration time of the spectrometer was set to 100 μs. The wavelengths were measured when the sensor was placed in both water and air. Compared with Fig. 4(b), no singular fringe peaks were observed as the noise of individual peaks shows much smaller variations. The variations in the average wavelengths with time are shown in Fig. 5(c), from which a noise level of 0.051 pm is obtained for the sensor in air and 0.052 pm for the sensor in water. The noise levels of the average wavelength are also indicated in Fig. 5(b), which is approximately four times smaller than the noises of the individual peaks. Using the experimentally-obtained temperature sensitivity of 84.6 pm/°C, a temperature resolution of ~6×10^{-4} °C is reached for the sensor. It is therefore demonstrated that the proposed average wavelength tracking method can also improve the sensor resolution for the case of no singular peaks, which manifests it as a universal method for wavelength tracking with reduced noise.

4. Response time

In addition to the high resolution discussed, fast response is another advantage of the proposed sensor. The response time can be characterized by monitoring the temperature transition when the sensor is quickly inserted into the medium of different temperature (warm water in our test case). In this section, the response time of this sensor is first theoretically studied via heat transfer analysis and then experimentally verified.

4.1 Heat transfer analysis

To give insights into how the sensor responses to the surrounding water temperature, the heat transfer process is briefly analyzed with a simplified model. The heat conduction between the surrounding water and the sensor as well as within the sensor is described by the heat equation give by [19]

$$\frac{\partial T}{\partial t} = \alpha \nabla^2 T, \tag{3}$$

where α is the thermal diffusivity of the sensor material and T is temperature. It can be seen from Eq. (3) that a large thermal diffusivity α is the key for temperature T to change rapidly. As a comparison, the thermal diffusivity of silicon is 8.8×10^{-5} m^2/s, which is more than 60 times larger than that for silica (1.4×10^{-6} m^2/s). Therefore, the proposed sensor based on silicon FP cavity in this paper will have a much faster response than those based on all-silica fiber temperature sensor.

It is difficult to directly solve Eq. (3) for the heat transfer analysis of the proposed sensor structure. However, the analysis can be greatly simplified using a lumped parameter model (LPM), where the temperature is assumed to be spatially uniform inside the silicon pillar. This assumption is justified by the small Biot number, B_i, of the sensor in water. The Biot number is defined as:

$$B_i = \frac{h \cdot L_c}{K_s}, \tag{4}$$

where L_c is the characteristic length of the sensor structure, K_s is the heat conductivity of silicon, and h is the heat transfer coefficient (HTC). A small Biot number (<< 1) implies that the heat conduction inside the silicon pillar is much faster than the heat transfer between the surrounding water and the pillar, resulting in negligible temperature gradient inside the silicon

#232621 - $15.00 USD Received 16 Jan 2015; revised 2 Mar 2015; accepted 4 Mar 2015; published 10 Mar 2015

pillar. The HTC, which denotes the amount of heat transfer from a unit temperature difference between the surrounding water and the sensor surface, can be calculated from [19]

$$h = \frac{N_u \cdot K_w}{L_c}, \tag{5}$$

where N_u is the Nusselt number for the water/silicon pillar surface, K_w is the heat conductivity of water. L_c is calculated as the ratio of volume of the silicon pillar to its surface areas that are exposed to the surrounding water. Using the experimental value $N_u = 1.2$ for water/silicon surface [20], and $K_w = 0.6\mathrm{W/(m \cdot K)}$, Eq. (5) gives $h = 3.96\times10^4\,\mathrm{W/(m^2 \cdot K)}$. Taking $K_s = 159\mathrm{W/(m \cdot K)}$, it can be calculated that $B_i = 4.5\times10^{-3}$ for the 80-μm-diameter and 200-μm-long silicon pillar. Since $B_i \ll 1$, it is verified that the LPM is valid for the sensor proposed here and used in water. The temperature of the silicon pillar, T, can be considered uniform within the silicon pillar and thus is only a function of time, as illustrated in Fig. 6(a). The change with time of the uniform temperature T within the whole lumped body is governed by a differential equation given as [19]

$$hA_s(T_\infty - T)dt = \rho_s C_s V_s dT, \tag{6}$$

where A_s is the surface area that exchanges heat, T_∞ is the temperature at steady state and, ρ_s, C_s, and V_s are, respectively, density, heat capacity and volume of the silicon pillar. For silicon, $\rho_s = 2.329\times10^3\,\mathrm{kg/m^3}$ and $C_s = 712\mathrm{J/(kg \cdot K)}$. Equation (6) indicates that the change in total heat within the silicon pillar is equal to the heat penetrating into the pillar from the silicon/water surface. Assuming the initial temperature of the silicon pillar is T_0, the solution to Eq. (6) is given as

$$T(t) = T_\infty + (T_0 - T_\infty)\exp\left(-\frac{hA_s}{\rho_s C_s V_s}t\right). \tag{7}$$

Equation (7) demonstrates that the temperature of the silicon pillar increases exponentially from its initial value to the steady state value. To facilitate comparison, we define the normalized temperature as

$$T_N(t) = \frac{T(t) - T_0}{T_\infty - T_0} = 1 - \exp\left(-\frac{hA_s}{\rho_s C_s V_s}t\right). \tag{8}$$

To demonstrate the influence of size of the silicon pillars on response time, the normalized temperature as a function of time has been calculated for several sensors with different parameters, the results are shown in Fig. 6(b). We define the response time (τ) of the sensor as the time when 63% (≈1-1/e) of the overall signal change is reached. From Eq. (8), τ is given by

$$\tau = \frac{\rho_s C_s V_s}{hA_s}. \tag{9}$$

Equation (9) along with the theoretical results in Fig. 6(b) indicate that a smaller and shorter silicon pillar has a quicker response time. This is expected because the smaller pillar has a larger surface-to-volume ratio that is advantageous for heat exchange. The response time of 0.76 ms for an 80-μm-diameter and 200-μm-length silicon pillar is thus obtained.

#232621 - $15.00 USD Received 16 Jan 2015; revised 2 Mar 2015; accepted 4 Mar 2015; published 10 Mar 2015

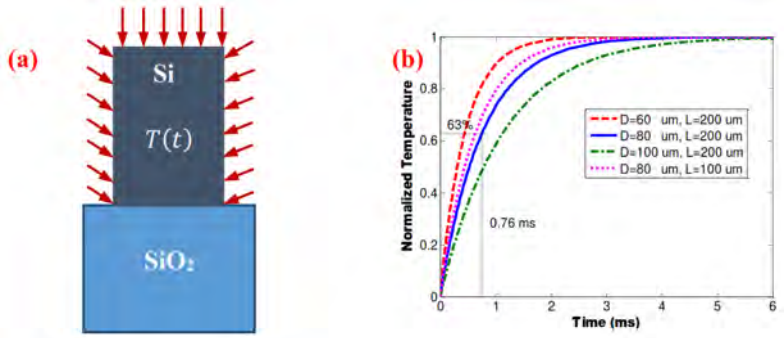

Fig. 6. (a) Lumped parameter model for heat transfer analysis of the sensor. (b) Simulated normalized temperature versus time for silicon pillars with different parameters. D and L denote diameter and length of the silicon pillar, respectively.

4.2 Experimental demonstration

The response time of the sensor was characterized by quickly inserting the sensor head at ambient temperature into a cup of hot water, as shown in Fig. 7(a). The spectral response to the heat transfer between the sensor head and the water was monitored by the high-speed spectrometer which was set at a frame rate of 6 kHz. Two sensors were fabricated and tested. The silicon pillar for one sensor has the diameter of 80 μm (red) and the other is 100 μm (black); both of them are 200 μm long. The average wavelength tracking method described in Section 3 was used for sensor demodulation. Figure 7(b) shows the average fringe peak wavelengths as a function of time for both sensors. It is evident that the response of each sensor shows two regions of different patterns. The average wavelength first experiences a relatively gradual wavelength increase followed by an abrupt and quick increase resembling the theoretical curves shown in Fig. 6(b). As the heat transfer between silicon and air is slower than that between the silicon and water, it is obvious that the region for the gradual wavelength increase corresponds to the process when the sensor was still in the air but approaching the water surface. Once the sensor was immersed in the water, the heat transfer was more rapid and the wavelength shift showed an abrupt increase. In Fig. 7(b), the time at the transition between the two regions is assumed to be 0. From these curves, the 63% rising times are found to be 0.51 ms for the sensor with 80-μm-diameter silicon pillar and 0.70 ms for the sensor with 100-μm-diameter silicon pillar. The sensor with the silicon pillar of smaller diameter has a faster response, which is consistent with the theoretical prediction shown in Fig. 6(b). The shorter response time in experiments than the theoretical value may arise from the underestimation of the HTC which is difficult to be accurately determined for our case. As a comparison, the response time of our sensor is much shorter than the experimental result of ~16 ms of a silica fiber coupler tip [9], in which the rising time is defined as the time needed when only 37% (≈1/*e*) of the overall signal change is reached.

Finally we note that the free spectral range (FSR) is ~1.46 nm, corresponding to a temperature range of ~17 °C, which is sufficient for many applications involving high-frequency temperature variations. By continuously tracking the fringe peaks during the measurement, measurement range much larger than a FSR can also be achieved. For example, in Fig. 7(a), the increase in temperature upon dipping the sensor into the hot water from air was about 33 °C (a wavelength shift of ~2 FSRs). The smooth transition of the measured temperature verifies that all peaks were successfully tracked even when the peak shift was greater than a FSR of the silicon FP cavity. When any of the peaks moves out of the wavelength range of the spectrometer, measurement error may occur due to the change in the set of fringe peaks used for averaging. By reducing the number of peaks for average wavelength tracking and using those peaks around the central wavelength of spectrometer, the

#232621 - $15.00 USD Received 16 Jan 2015; revised 2 Mar 2015; accepted 4 Mar 2015; published 10 Mar 2015

temperature measurement range can be greatly increased. However, this will also lead to reduced SNR because fewer peaks are being used for averaging.

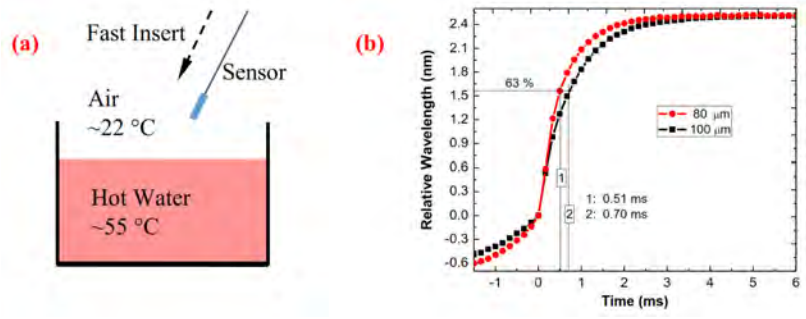

Fig. 7. (a) The response time is measured by fast insertion into hot water. (b) Experimental relative wavelength versus time.

5. Conclusion

This paper demonstrates a fast-response fiber-optic temperature sensor based on a silicon pillar attached on the endface of a SMF that forms a FP cavity. Due to the high transparency and large RI of silicon material over infrared wavelength range, a fringe visibility as high as 33 dB around wavelength of 1550 nm was obtained for the FP cavity. The relatively long length of the silicon pillar and the large RI of silicon also lead to a short FSR and a large number of fringes in spectral range of the demodulation system for the sensor.

Exploiting the availability of multiple fringes, we have proposed and demonstrated a novel average wavelength tracking method for the sensor signal demodulation. This method is shown to be capable of suppressing the potential singular fringe peaks that have extra-large noise due to limited data points, which is often associated with high-speed spectrometers. For spectral frames without singular fringe peaks, the method also significantly improves the measurement resolution by reducing the random noise from the average effect. Using this novel average wavelength tracking method, a wavelength noise as low as ~0.05 pm in both air and water is experimentally obtained. Using the experimentally-obtained temperature sensitivity of 84.6 pm/°C, the sensor has a temperature resolution of 6×10^{-4} °C.

The high thermal diffusivity of silicon and the small size of sensor head endow the sensor with a fast response to the temperature change. A response time as short as 0.51 ms is obtained for an 80-μm-diameter and 200-μm-long silicon pillar in water, indicating a maximum frequency of ~2 kHz can be reached for temperature sensing.

Acknowledgments

This work was partially supported by U.S. Naval Research Laboratory under contract no. N0017315P0376. The fabrication of silicon pillars was carried out in the Minnesota Nano Center which receives partial support from NSF through the NNIN program. We thank Prof. Zhaoyan Zhang for stimulating discussions on the heat-transfer problem and Mr. Dustin Dam for technical support on the high-speed spectrometer.